REALTIME COMPUTATION OF WALL SHAPES IN A TWO-DIMENSIONAL ADAPTIVE TEST SECTION

Dr. H. Holst, DLR Göttingen, Federal Republic of Germany

Summary

By adapting solely top and bottom flexible walls of a solid-walled test section of rectangular cross section it can be achieved that the wall interferences (Mach number correction, angle of attack correction) are zero along the test section centreline, when testing three-dimensional models. The shapes of the flexible top and bottom walls are determined by the well known Wedemeyer/Lamarche method of two-dimensional wall adaptation for three dimensional models.

The method performs the wall shape determination in a single computational step, at least when starting from the wall shapes of a preceding Mach number or angle of attack.

It uses - in the original computer code of Lamarche - a numerical representation of the necessary mathematical operators. The computing time of 17 seconds on a personal computer could be reduced to 0.3 seconds by using an analytical representation of the operators - following a proposal of E. Wedemeyer. This facilitates the development of a high productivity strategy for wall adaptation in the modernized transonic facility of DLR Göttingen, which is equipped with a two-dimensional adaptive test section of 1.0 m × 1.0 m.

List of symbols

β	transonic parameter, $\beta = \sqrt{1 - M^2}$
B	width of test section
δ_0	lift interference parameter
Δn	wall displacement
φ	velocity potential
H	height of test section
L	length of test section
Λ	mathematical operator
M	Mach number
τ	blockage interference parameter
u^u	measured velocity on upper wall
u^l	measured velocity on lower wall
u^A	antisymmetrical component of velocity
u^S	symmetrical component of velocity
U_∞	free stream velocity
u^{int}	longitudinal interference velocity
w^{int}	vertical interference velocity
x, y, z	cartesian coordinates
ξ, η, ζ	cartesian coordinates
X	mathematical operator

Subscripts

M	model
wall	measured value at the wall
wing	lifting wing
∞	undisturbed flow

Superscripts

A	antisymmetric
int	interference
l	lower wall
S	symmetric
u	upper wall

1. Introduction

After some experiences with two-dimensional wall adaptation for three-dimensional measurements in the test section of the high speed wind tunnel of DLR Göttingen [1], it was decided to equip the transonic facility of DLR Göttingen with a top-and-bottom-flexible-walled test section in the course of modernization. The so called Wedemeyer/Lamarche-method [2] was to be used for wall adaptation. So the computing times necessary for determining the wall contours of top and bottom walls of about 17 seconds on a personal computer were unacceptable. A method had to be found to drastically reduce the computing time and facilitate at least near real time conditions of determining the wall shapes.

2. Two – dimensional wall adaptation for three – dimensional measurements

By two-dimensional wall adaptation for three-dimensional models it can be achieved that the wall interferences on the centreline of the test section are zero. That makes it easier to correct the experimental data, e.g. the pitching moment correction.

It is assumed that the Prandtl-Glauert approximation can be applied, linear theory is valid, so the superposition principle is valid.

Making use of the image technique, the wall interferences on the test section centreline can be related to the measured wall pressures on the centrelines of the top and bottom flexible walls. Wall deformations can be computed, which just cancel the centreline wall interferences u^{int} and w^{int}, which are "responsible" for blockage and angle-of-attack corrections respectively. The details of the method are given in [3] and [4].

To demonstrate what is the capability of two-dimensional wall adaptation in three-dimensional flow, **Fig. 1** shows the well known blockage interference factor τ [5] as a function of the lateral coordinate y (spanwise direction). The shaded region indicates the amount of residual wall interference and its spanwise distribution. Not only in this section ($x = x_{wing}$), but everywhere along the centreline, the wall interference can be eliminated by adapting only top and bottom flexible walls.

Fig. 2 shows a similar diagram for the case of upwash interference. Again it can be observed that the wall interference is substantially alleviated by two-dimensional wall adaptation. The residual wall interference is extremely small along the quarter chord line of the wing for a sweep angle of 26° in a test section with a "close to square" cross section. These data have been generated by application of the image technique and "compressible" singularities, according to the Prandtl-Glauert transformation [4].

3. Measurements in a two – dimensional adaptive wall test section

In 1987 measurements have been carried out, in the Göttingen high speed wind tunnel using the Laval nozzle with top and bottom flexible walls for two-dimensional wall adaptation. The test section height is

$$H = 0.670\ m\ ,$$

its width is

$$B = 0.725\ m\ ,$$

and its length is

$$L = 2.200\ m\ .$$

The high speed wind tunnel is a blow down facility with maximum testing time of about 40 sec at M = 0.7.

The model is shown in **Fig. 3**. It was placed at the centre of the test section, $x_M = 0.5\ L$. The method could be validated [1], results of wall contours are given later, when comparing the "old" and "new" methods for wall adaptation.

From this successful application of the method, the decision was taken to equip the transonic facility of DLR Göttingen with a two-dimensional adaptive wall test section.

This test section has a height of

$$H = 1.0\ m\ ,$$

and a width of

$$B = 1.0\ m\ .$$

Its the length is

$$L = 4.510\ m\ .$$

Top and bottom walls are flexible and adjustable by 22 and 20 jacks respectively. The accuracy of wall setting could be realized within 0.1 mm, the test section is computer controlled and can be operated fully automatically.

The computing time of the "old" Wedemeyer/Lamarche wall adaptation procedure (using a numerical representation of the mathematical operators X [Chi] and Λ [Lambda] for blockage and lift influences respectively) of about 17 sec on a personal computer was no longer acceptable.

Wall shape prediction methods had to be developed to achieve acceptable productivity. To this end Wedemeyer [6] proposed to approximate the operators X and Λ by analytical expressions, herewith to evade the time consuming numerical computations. It will be demonstrated in the following how accurately the operators X and Λ are represented by the analytical formulae.

4. Determination of the wall shapes

The wall pressure distribution of the centre-lines of top and bottom walls gives the distribution of the corresponding longitudinal velocities via the relationship

$$\frac{u}{U_\infty} = -\frac{c_p}{2} \qquad (1)$$

which is also valid for compressible subsonic flow, when the Prandtl-Glauert rule can be applied.

This distribution can be decomposed in a symmetrical part caused by blockage and an antisymmetrical part caused by lift. Both parts are treated separately and the results are then superimposed. This is permitted because of the linearity assumed. The decomposition is given in the following for the symmetrical blockage part

$$u^S = \frac{1}{2}(u^u + u^l) \qquad (2)$$

and for the antisymmetrical lift part

$$u^A = \frac{1}{2}(u^u - u^l) \qquad (3)$$

The wall displacement for blockage is then given by

$$\frac{\Delta n^S(x)}{H} = \int_{-\infty}^{+\infty} u^S{}_{wall}(x-\eta)\, \mathrm{X}(\eta)\, d\eta \qquad (4)$$

and for lift it is given by

$$\frac{\Delta n^A(x)}{H} = \int_{-\infty}^{+\infty} u^A{}_{wall}(x-\eta)\, \Lambda(\eta)\, d\eta \qquad (5)$$

At the beginning - as part of the calibration - the areodynamically straight wall shapes are determined. For the slightly divergent test section (compensation of boundary layer displacement thickness growth) the wall pressure distribution of the empty test section should be zero. Residual variations of the pressure distribution are attributed to pressure orifice individualities and corrected for, before starting with the evaluation and the computation of the wall shapes. The walls with their already existing wall displacements (deviations from geometrically straight) are regarded as straight, they are called *aerodynamically straight*, and are the starting point.

When there are wall displacements e.g. from a preceding wall adaptation (that is *normally* the case), they are accounted for by using approximate formulae, derived from a power series expansion of the disturbance potential that results from the wall deflection. Thus the wall pressure distribution is reduced to the straight wall conditions, and equations (4) and (5) can be applied [7].

5. New method for representation of the operators X, Λ

The operators X and Λ can be represented by simple approximation formulae proposed by Wedemeyer [8]. For blockage the operator X is given by

$$X(y) = \frac{E}{4}\left\{\frac{1}{[E+y^2]^{\frac{3}{2}}}\left(1+\frac{E-4y^2}{8(E+y^2)^2}\right)\right\} \quad (6)$$

where E was found to be best with a value of

$$E = 0.3806 \ .$$

The operator for lift, namely Λ, is given by the following equation:

$$\Lambda(y) = E_1\left[y-\sqrt{E_2+y^2}\right] + E_4\left[\sqrt{E_3+y^2}-\sqrt{E_2+y^2}\right] \quad (7)$$

where

$$E_4 = \frac{0.084 + E_1\cdot\sqrt{E_2}}{\sqrt{E_3}-\sqrt{E_2}} \quad (8)$$

with the factors E_1 to E_4:

$$E_1 = 0.4740$$

$$E_2 = 0.0813$$

$$E_3 = 0.0697$$

$$E_4 = 10.2300 \ .$$

The analytical interpolation formulae for X and Λ are designed so that the asymptotic behaviour for $y \to \pm\infty$ and certain integral values are correctly represented. The values of E and E_1 to E_4 are determined by a curve fitting procedure. **Fig. 4** and **Fig. 5** show comparisons of the Lamarche numerical solution for the operators X and Λ taken from [3] and the interpolation formulae (6) and (7), see also **Table 1** and **Table 2**. A good agreement can be observed. The values for E and E_1 to E_4 are valid for test sections with cross sections "close to square", i.e. for ratios H/B from about 0.80 to 1.25.

6. Evaluation of measurements

Measurements were re-evaluated, using the "old" as well as the "new" method. **Fig. 6** shows the two contributions to the wall deflections (symmetrical for blockage and antisymmetrical for lift) computed by the old and the new method.

It can be seen that the results agree quite well, which proves that the new method is valid. The differences at the end of the test section are due to different extrapolations of the pressure data at the end of the test section. The contours of top and bottom walls are given in **Fig. 7**, again showing perfect agreement.

The residual wall interferences (w^{int}, lift) were evaluated using a method based on measured wall pressures applying Green's theorem [8]. The result is given in **Fig. 8** and indicates that the walls should have been deflected further downwards than it was during the measurements. This is also suggested by the wall contours given by the new method.

It should be pointed out that - by representing the operators analytically - some difficulties of the "classical" Wedemeyer/Lamarche

method (i.e. the computer code) can be avoided. This is demonstrated by the last two figures. **Fig. 9** shows accuracy problems of the antisymmetrical wall deflection, when the origin of the coordinate system is not placed "where the lift happens". The origin of the coordinate system should be placed e.g. at the quarter chord line of the wing. For the new method the results are not affected by the choice of the coordinate system.

Fig. 10 shows that under certain conditions the symmetrical wall displacements (due to blockage) do behave unstable. This did never happen with the new method, which is, therefore, more reliable.

The operators X and Λ are given in **Table 1** and **Table 2**. Note that the operator Λ is plotted with the sign of the coordinate η inverted.

7. Concluding remarks

A new method for wall shape determination in a two-dimensional adaptive wall test section for three-dimensional measurements is presented. The mathematical operators needed could be approximated by formulae proposed by Wedemeyer. The computing time could drastically be reduced - by a factor of 50 to presently 0.3 sec on a personal computer - thus facilitating a near real time operation of the adaptive test section of the transonic wind tunnel of DLR Göttingen.

8. References

(1) Holst, H., Raman, K.S.
2-D Adaptation for 3-D Testing.
DLR-IB 29112-88 A 03, DLR Göttingen, Germany, 1988.

(2) Wedemeyer, E.
Wind Tunnel Testing of Three-Dimensional Models in Wind Tunnels with Two Adaptive Walls.
Technical Note 147, von Kármán Institute for Fluid Dynamics, Brussels, Belgium, 1982.

(3) Lamarche, L., Wedemeyer, E.
Minimization of Wall Interference for Three Dimensional Models with Two Dimensional Wall Adaptation.
Technical Note 149, von Kármán Institute for Fluid Dynamics, Brussels, Belgium, 1984.

(4) Wedemeyer, E.
The Computer in Experimental Fluid Dynamics.
Lecture Series1986-06, von Kármán Institute for Fluid Dynamics, Brussels, Belgium, 1985.

(5) Garner, H.G., Rogers, E.W.E, Acum, W.E.A., Maskell, E.C.
Subsonic Wind Tunnel Wall Corrections.
AGARDograph 109, 1966.

(6) Wedemeyer, E.
Private communication.
Göttingen, Nov. 1992.

(7) Wedemeyer, E.
Adaptive Wind Tunnel Walls: Technology and Applications. (Section 4: Testing of 3-D models in 2-D adaptive wall test sections.)
AGARD-AR-269, April 1990.

(8) Holst, H.
Procedure for Determination of Three-Dimensional Wind Tunnel Wall Interferences and Wall Adaptation in Compressible Subsonic Flow Using Measured Wall Pressures.
DLR-FB 91-09, DLR, Göttingen, Germany, 1991.

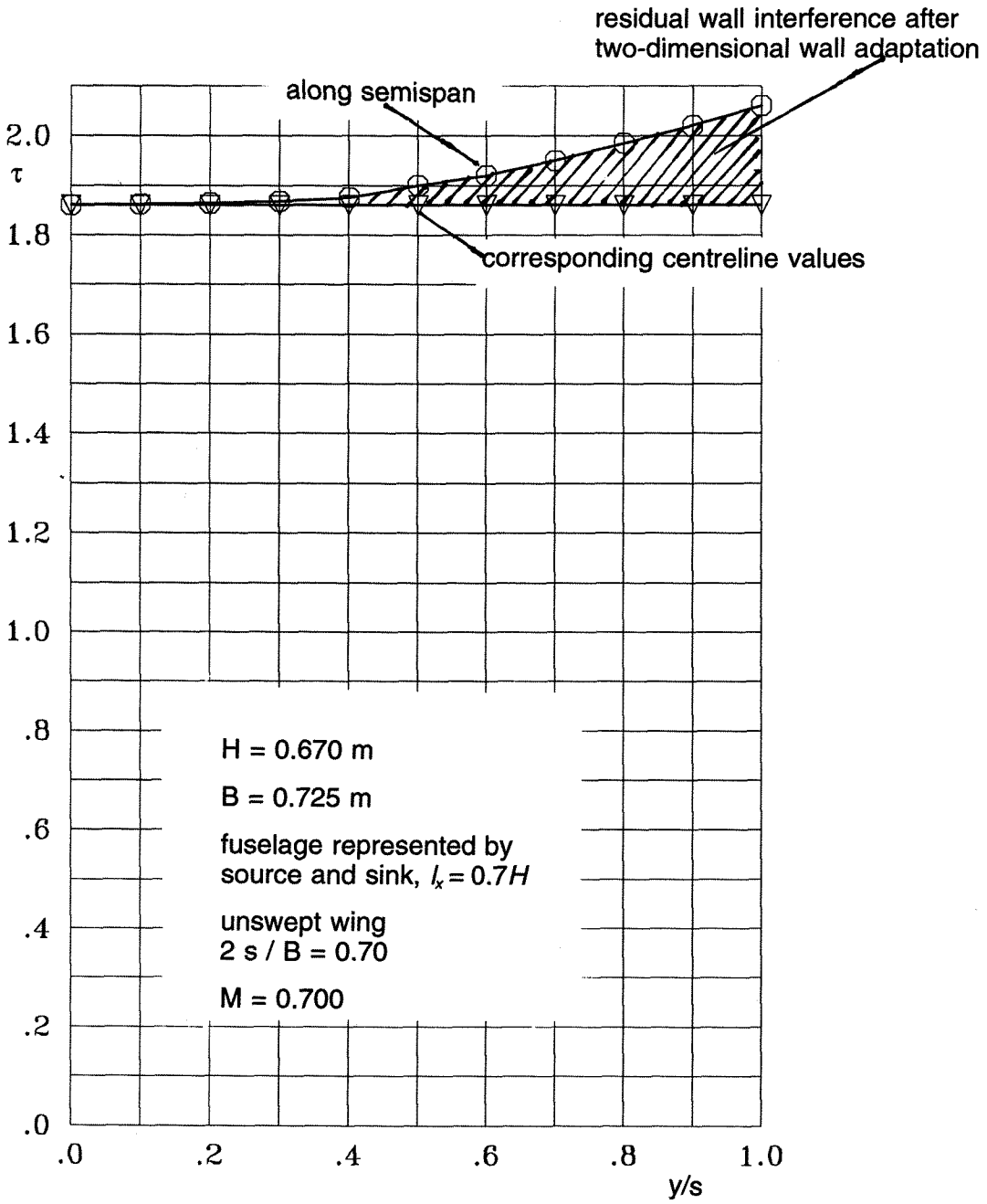

Fig. 1:

Blockage interference factor τ in a test section of rectangular cross section. Shaded region indicates residual wall interference after two-dimensional wall adaptation of top and bottom flexible walls.

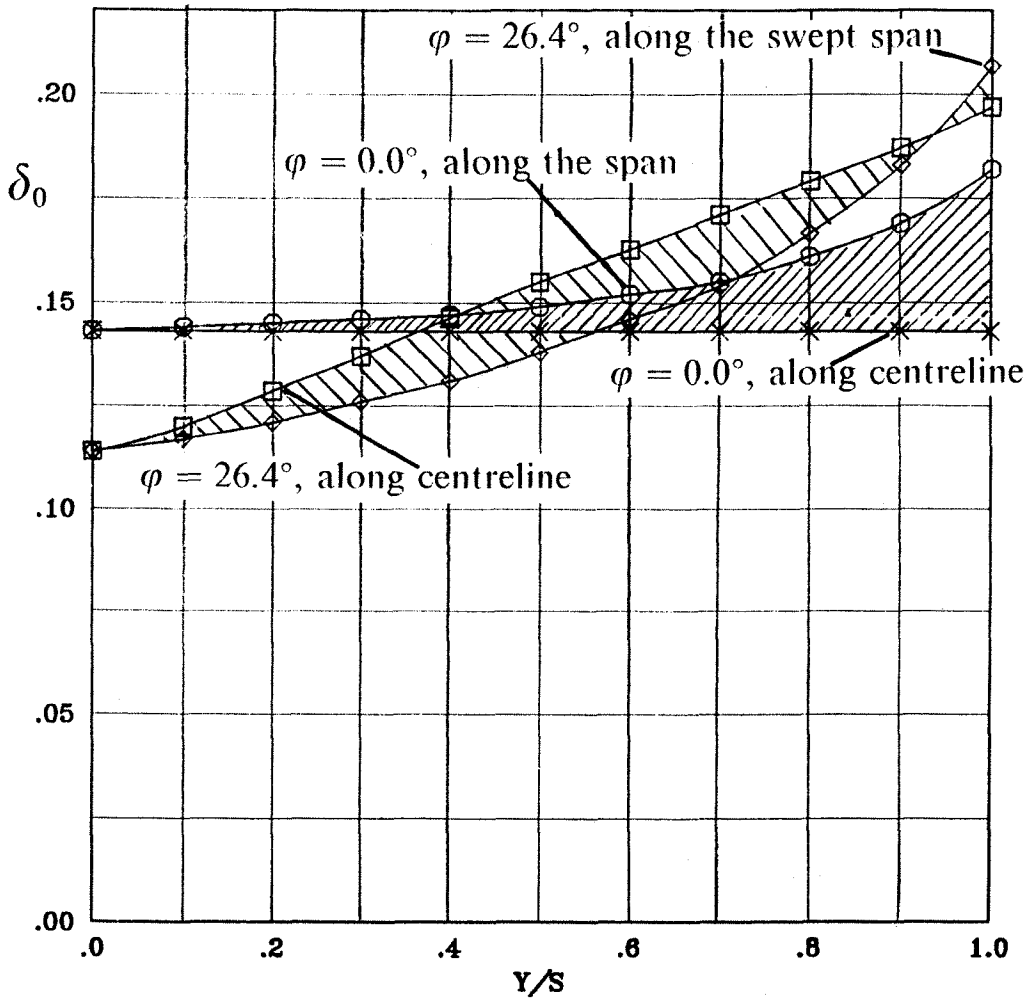

Fig. 2:

Expected residual wall interference δ_0 for a straight wing and a wing of 26.4° sweep back angle. Shaded region indicates residual wall interference after two-dimensional wall adaptation of top and bottom flexible walls.

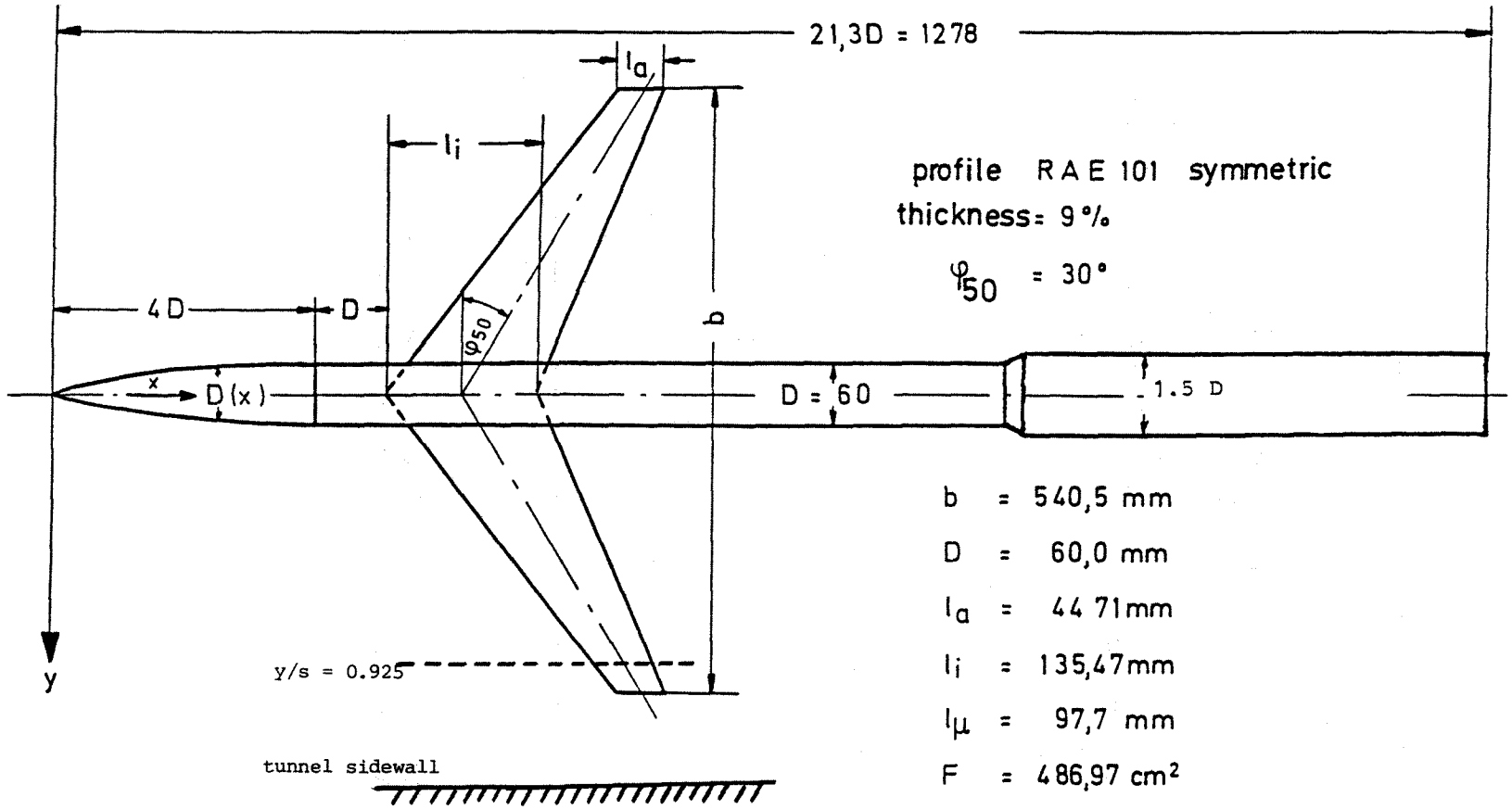

Fig. 3:

Details of lift model. Sidewall relative to the wing tip is indicated.

b = 540,5 mm

D = 60,0 mm

l_a = 44 71mm

l_i = 135,47mm

l_μ = 97,7 mm

F = 486,97 cm²

Λ = 6

λ = 0,33

$$\frac{D(x)}{D} = 2\left[\frac{1}{3}\left(\frac{x}{D}\right) - \left(\frac{1}{16}\right)\left(\frac{x}{D}\right)^2 + \frac{1}{1536}\left(\frac{x}{D}\right)^4\right]$$

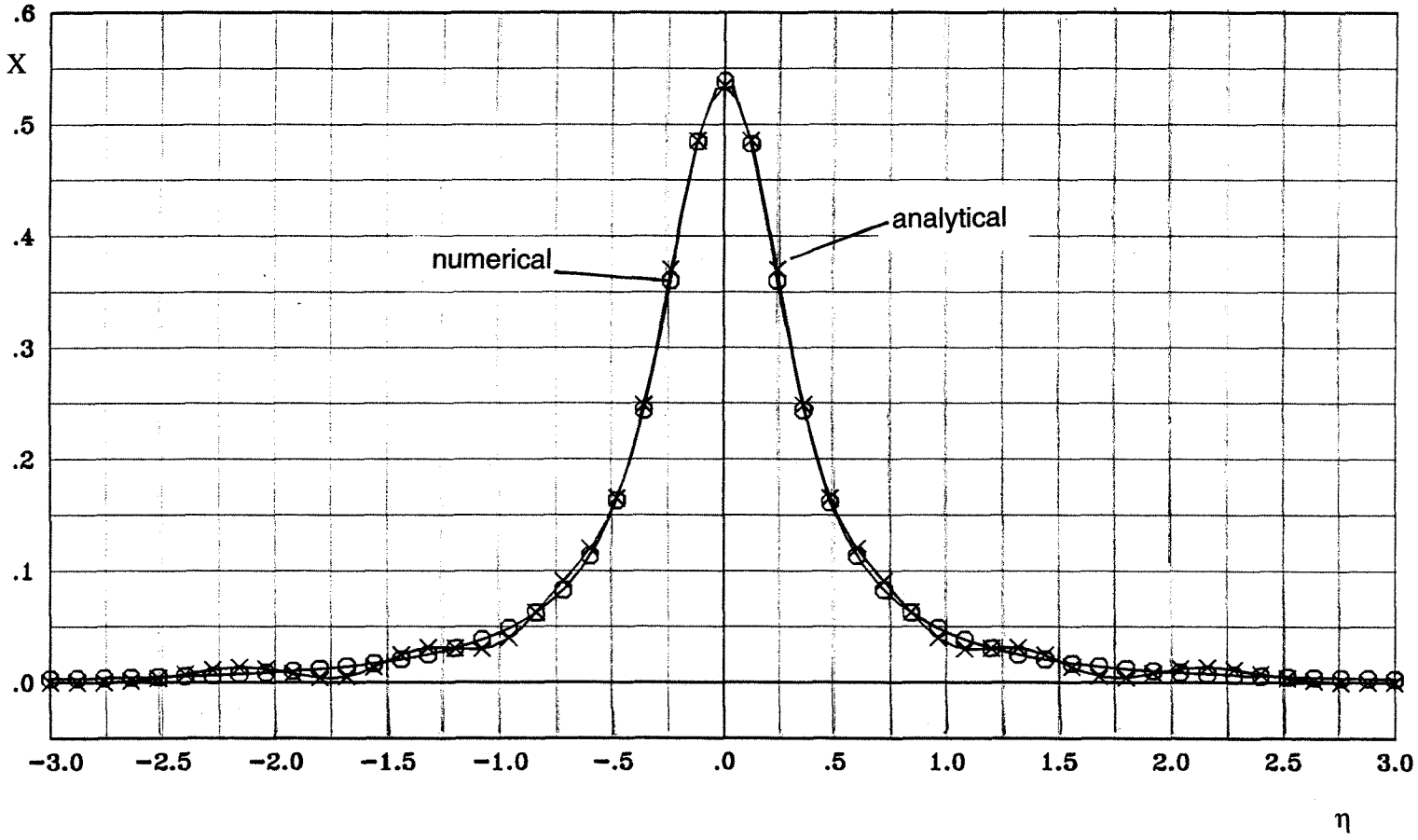

Fig. 4:

Operator X(η), comparison of the two different solutions.

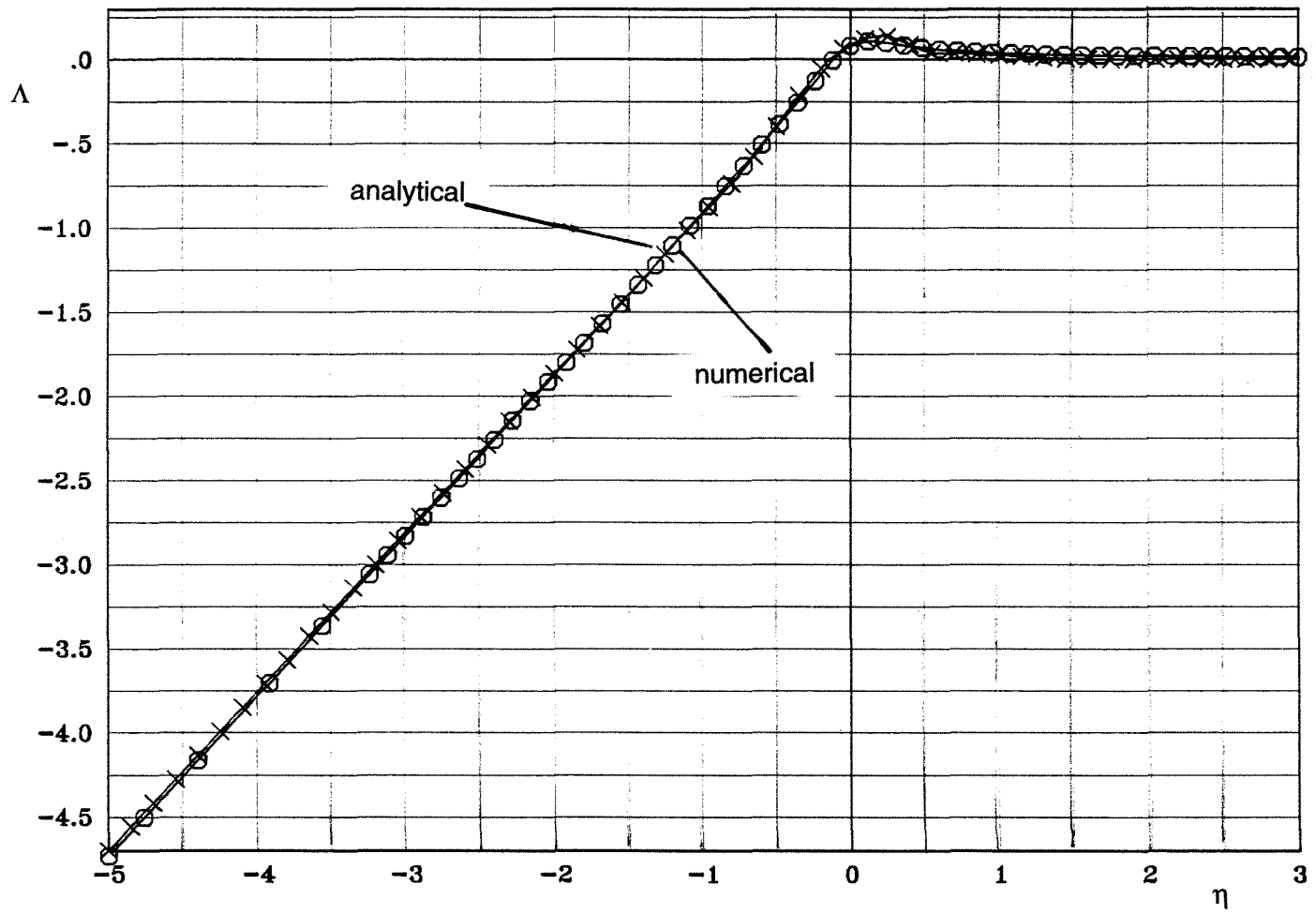

Fig. 5:

Operator $\Lambda(\eta)$, comparison of the two different solutions.

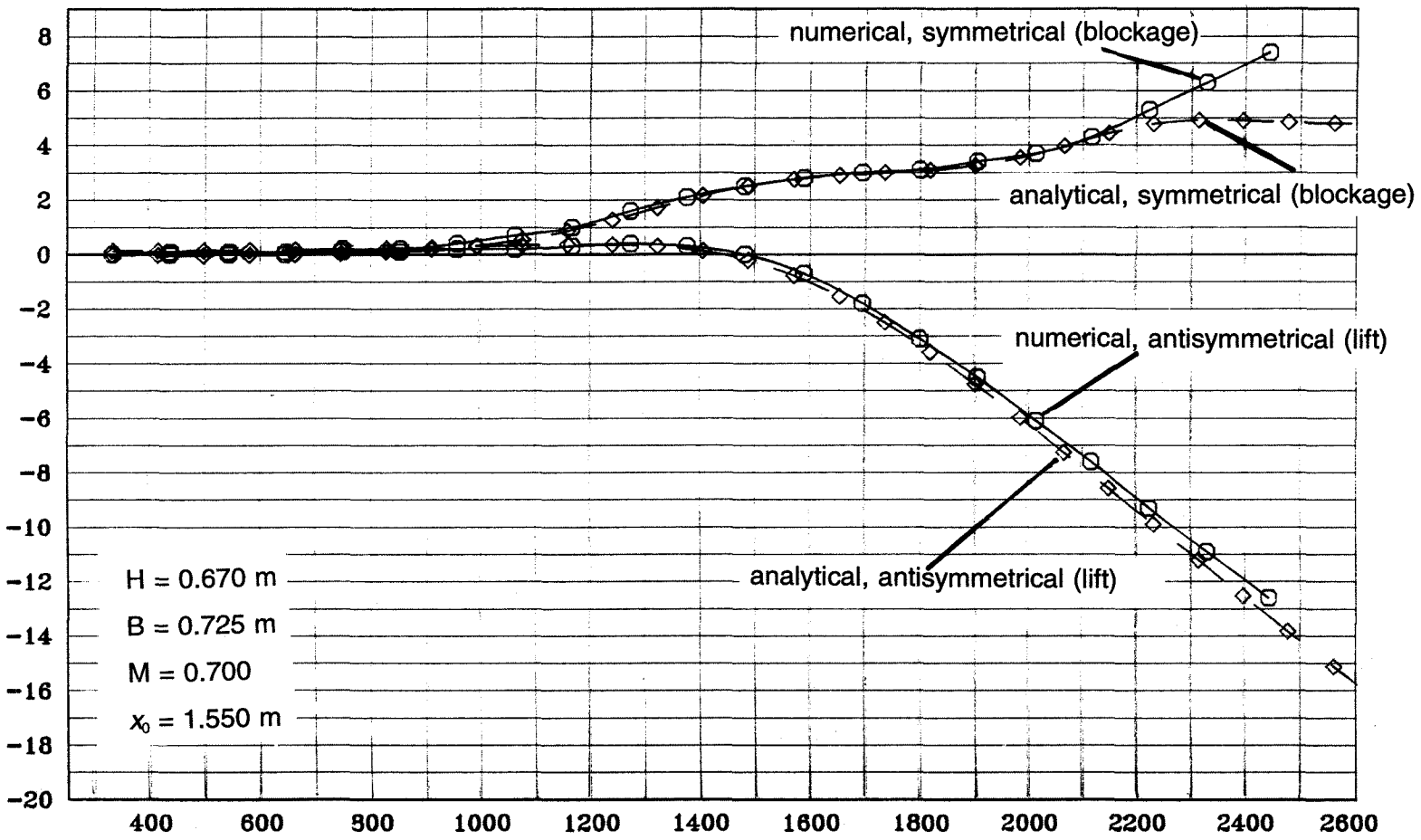

Fig. 6:

Symmetrical and antisymmetrical contributions to wall displacement, comparison of the "old" and the "new" methods.

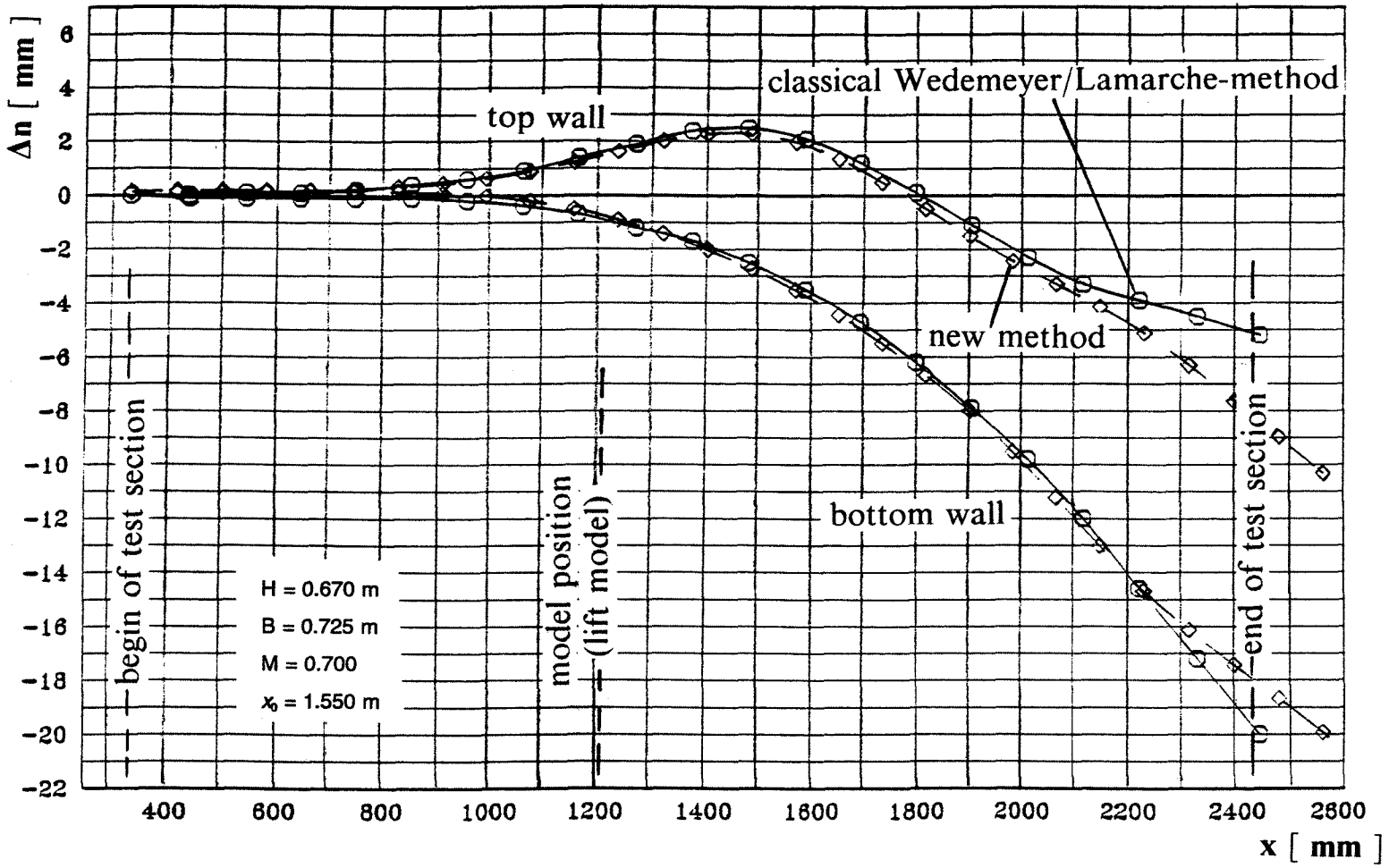

Fig. 7:

Comparison of wall shapes.

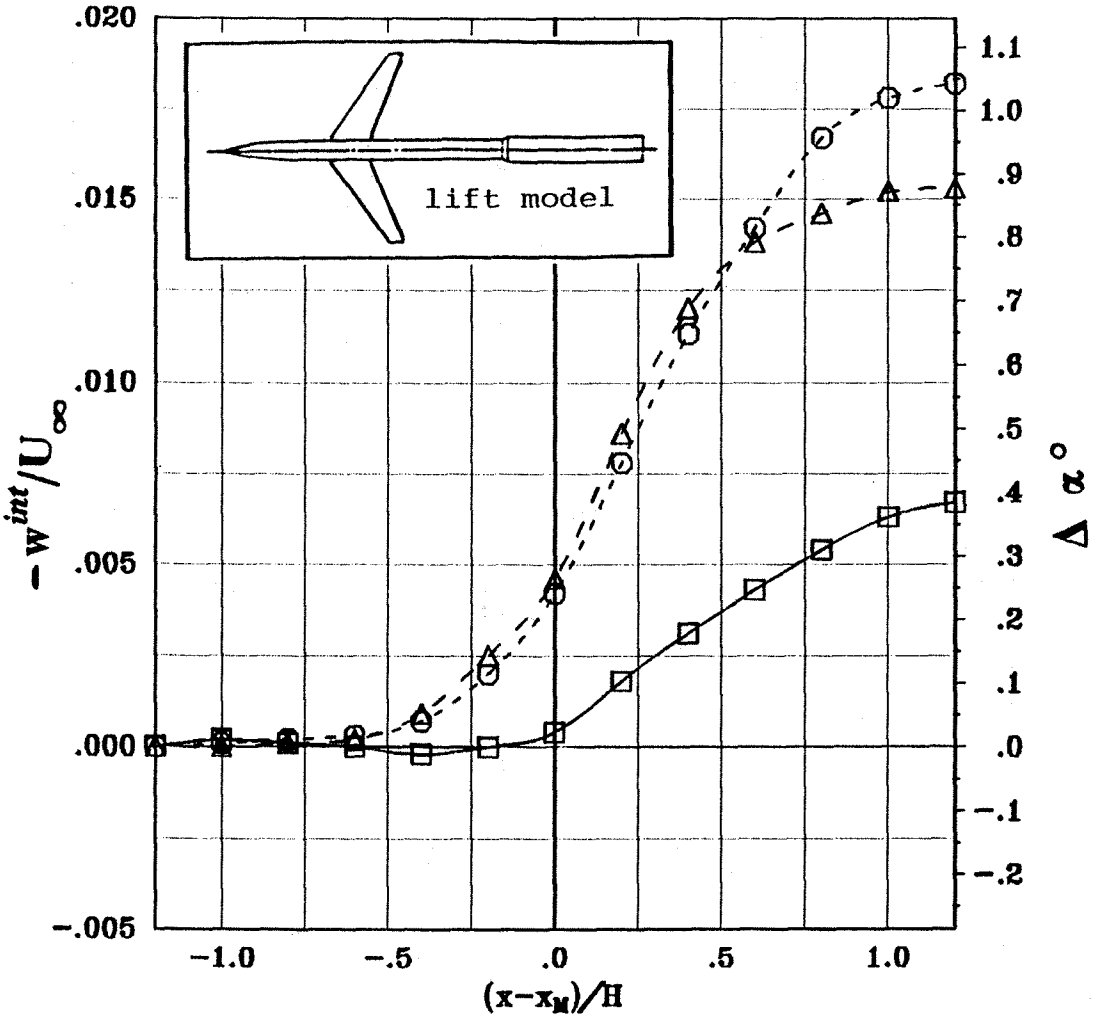

Fig. 8:

Interferences and residual interferences w^{int} along the test section centreline and corresponding angle of attack corrections $\Delta\alpha$ for the swept wing model.

$M = 0.704$	Mach number
$\alpha = 6°$	angle of attack
$b/B = 0.75$	relative spanwidth
$\varphi = 30°$	sweep back angle
$H = 0.670m$	height of test section
$B = 0.725m$	width of test section

Δ Interferences for aerodynamically straight walls, method of images
o aerodynamically straight walls, interferences computed using a wall pressure method
□ two-dimensionally adapted walls according to Wedemeyer/Lamarche, residual interferences computed according to [8]

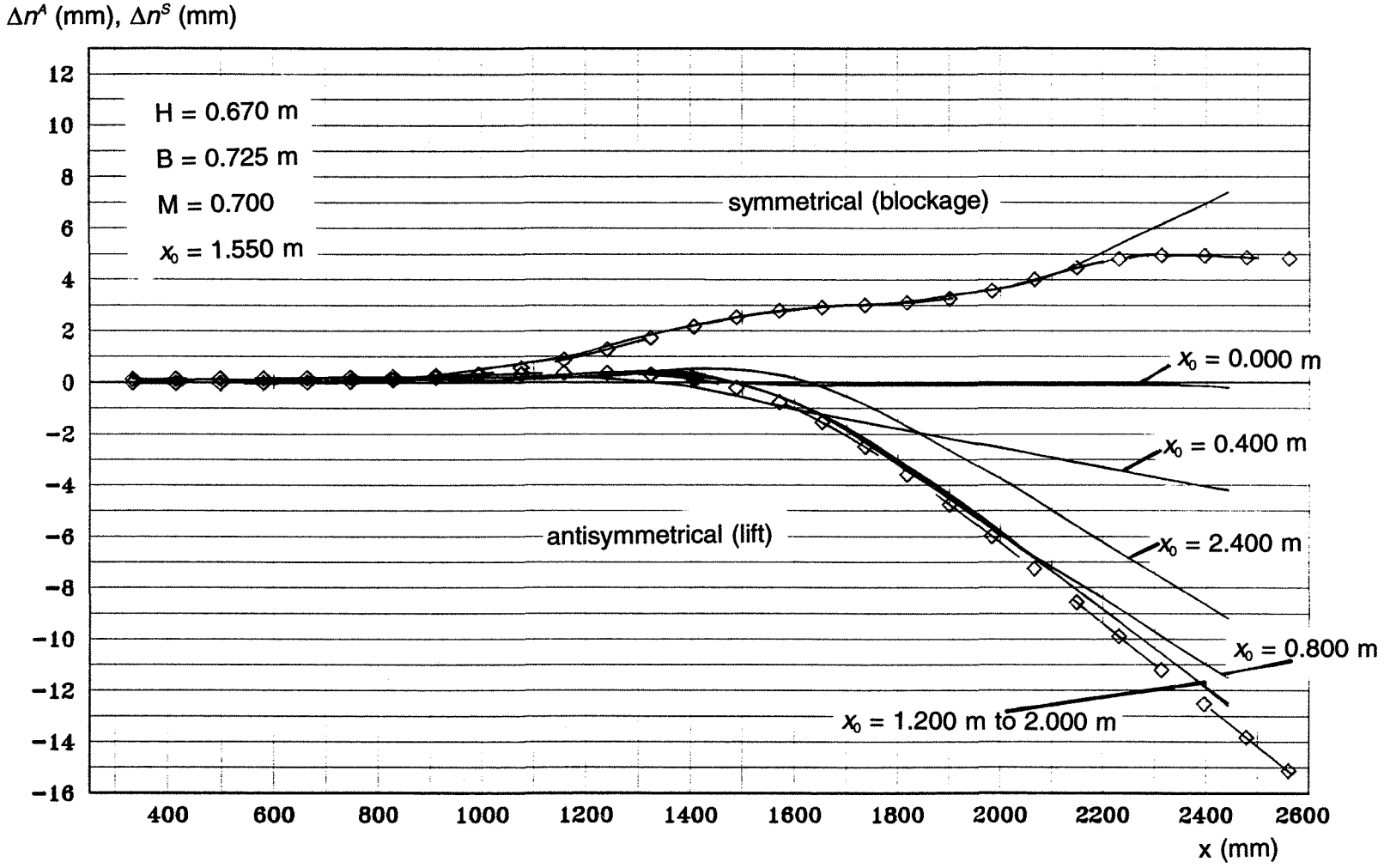

2751

Fig. 9:

Accuracy problems depending on choice of the coordinate system for the "old" method.

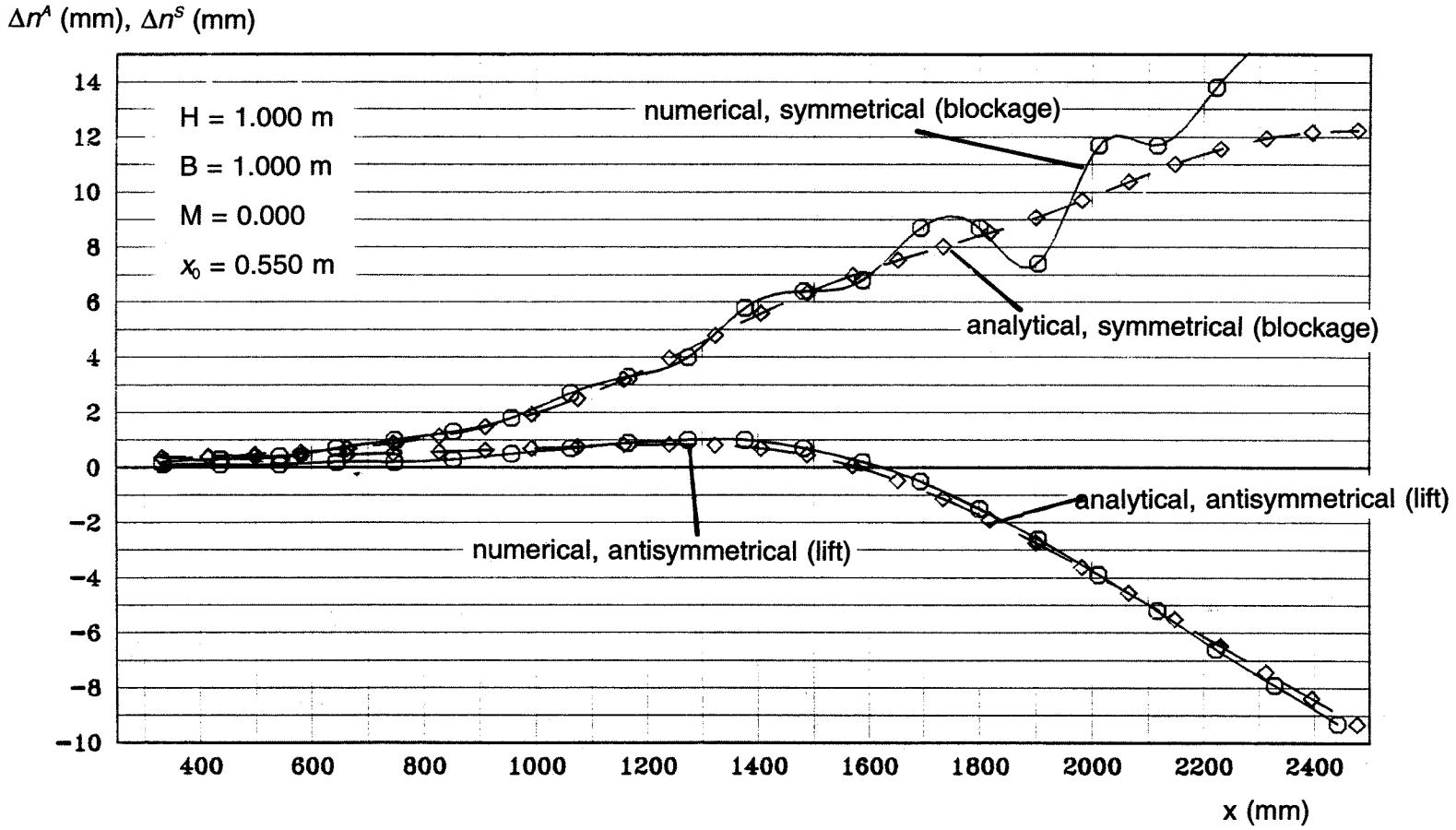

Fig. 10:

Oscillatory solution under certain conditions for the "old" method.

i	η	X_{old}	X_{new}
1	-3.00	0.00000	0.00314
2	-2.88	0.00000	0.00352
3	-2.76	0.00022	0.00396
4	-2.64	0.00148	0.00471
5	-2.52	0.00393	0.00507
6	-2.40	0.00751	0.00578
7	-2.28	0.01126	0.00663
8	-2.16	0.01339	0.00764
9	-2.04	0.01225	0.00886
10	-1.92	0.00815	0.00103
11	-1.80	0.00441	0.01215
12	-1.68	0.00566	0.01439
13	-1.56	0.01376	0.01718
14	-1.44	0.02467	0.02068
15	-1.32	0.03120	0.02514
16	-1.20	0.03076	0.03087
17	-1.08	0.03014	0.03838
18	-0.96	0.03987	0.04843
19	-0.84	0.06255	0.06230
20	-0.72	0.09056	0.08239
21	-0.60	0.12004	0.11324
22	-0.48	0.16516	0.16133
23	-0.36	0.24865	0.24381
24	-0.24	0.36983	0.36010
25	-0.12	0.48550	0.48247
26	-0.00	0.53387	0.53835
27	+0.12	0.48552	0.48248
28	+0.24	0.36985	0.36010
29	+0.36	0.24864	0.24382
30	+0.48	0.16514	0.16313
31	+0.60	0.12003	0.11324
32	+0.72	0.09057	0.08239
33	+0.84	0.06256	0.06230
34	+0.96	0.03988	0.04843
35	+1.08	0.03014	0.03838
36	+1.20	0.03075	0.03087
37	+1.32	0.03119	0.02513
38	+1.44	0.02467	0.02068
30	+1.56	0.01377	0.01718
40	+1.68	0.00567	0.01439
41	+1.80	0.00441	0.01215
42	+1.92	0.00815	0.01034
43	+2.04	0.01225	0.00886
44	+2.16	0.01339	0.00764
45	+2.28	0.01126	0.00663
46	+2.40	0.00751	0.00578
47	+2.52	0.00393	0.00507
48	+2.64	0.00148	0.00447
49	+2.76	0.00022	0.00395
50	+2.88	0.00000	0.00352
51	+3.00	0.00000	0.00314

Table 1:

Operator $X(\eta)$, comparison of old and new solution.

i	η	Λ_{old}	Λ_{new}
1	-2.50	+0.00000	+0.01591
2	-2.35	+0.00000	+0.01691
3	-2.20	+0.00000	+0.01840
4	-2.05	+0.00000	+0.01933
5	-1.90	+0.00000	+0.02082
6	-1.75	+0.00068	+0.02255
7	-1.60	+0.00272	+0.02460
8	-1.45	+0.00609	+0.02704
9	-1.30	+0.01094	+0.03001
10	-1.15	+0.01717	+0.03368
11	-1.00	+0.02432	+0.03832
12	-0.85	+0.03159	+0.04436
13	-0.70	+0.03773	+0.05243
14	-0.55	+0.04116	+0.06356
15	-0.40	+0.08953	+0.07904
16	-0.25	+0.13857	+0.09851
17	-0.10	+0.12490	+0.10721
18	+0.05	+0.06435	+0.05168
19	+0.20	-0.05366	-0.08524
20	+0.35	-0.21556	-0.24652
21	+0.50	-0.39749	-0.40582
22	+0.65	-0.57571	-0.56045
23	+0.80	-0.73614	-0.71162
24	+0.95	-0.87835	-0.86044
25	+1.10	-1.01530	-1.00769
26	+1.25	-1.15578	-1.15386
27	+1.40	-1.29752	-1.29923
28	+1.55	-1.43926	-1.44403
29	+1.70	-1.58101	-1.58340
30	+1.85	-1.72275	-1.73242
31	+2.00	-1.86450	-1.87619
32	+2.15	-2.00624	-2.01975
33	+2.30	-2.14798	-2.16313
34	+2.45	-2.28973	-2.30637
35	+2.60	-2.43147	-2.44949
36	+2.75	-2.57322	-2.59252
37	+2.90	-2.71496	-2.73546
38	+3.05	-2.85670	-2.87832
30	+3.20	-2.99845	-3.02113
40	+3.35	-3.14014	-3.16389
41	+3.50	-3.28193	-3.30659
42	+3.65	-3.42368	-3.44926
43	+3.80	-3.56542	-3.59189
44	+3.95	-3.70717	-3.73448
45	+4.10	-3.84891	-3.87705
46	+4.25	-3.99065	-4.01960
47	+4.40	-4.13240	-4.16211
48	+4.55	-4.27414	-4.30461
49	+4.70	-4.41589	-4.44710
50	+4.85	-4.55763	-4.58960
51	+5.00	-4.69937	-4.73202

Table 2:

Operator $\Lambda(\eta)$, comparison of old and new solution.